# Binding of biological effectors on magnetic nanoparticles measured by a magnetically induced transient birefringence experiment

C. Wilhelm,[1] F. Gazeau,[1] J. Roger,[2] J. N. Pons,[2] M. F. Salis,[2] R. Perzynski,[1] and J. C. Bacri[1]

[1]*Laboratoire des Milieux Désordonnés et Hétérogènes, Université Pierre et Marie Curie, Tour 13, Case 86, 4 place Jussieu, 75252 Paris Cedex 05, France and UFR de Physique, Université Paris 7-Denis, Diderot, France*

[2]*Laboratoire des Liquides Ioniques et Interfaces Chargées, Université Pierre et Marie Curie, Bâtiment F, Case 63, 4 place Jussieu, 75252 Paris Cedex 05, France*

(Received 21 June 2001; revised manuscript received 11 September 2001; published 19 February 2002)

We have investigated the relaxation of the magnetically induced birefringence in a suspension of magnetic nanoparticles in order to detect the binding reaction of polyclonal antibodies on the particle surface. The birefringence relaxation is driven by the rotational diffusion of the complex formed by the magnetic nanoparticles bound to the antibody and thus is directly related to the hydrodynamic size of this complex. Birefringence relaxations are well described by stretched exponential laws revealing a polydisperse distribution of hydrodynamic diameters. Comparing the size distribution of samples with different initial ratios of immunoglobuline added per magnetic nanoparticles, we evidence the graft of an antibody on particle and eventually the onset of particles agregation. Measurements on samples separated in size by gel filtration demonstrate the robustness of our experiment for the determination of size distribution and its modification due to the adsorption of a macromolecule. The immunoglobuline binding assay is performed comparatively for ionic magnetic nanoparticles with different coatings.

DOI: 10.1103/PhysRevE.65.031404 PACS number(s): 82.70.Dd, 75.50.Mm, 78.20.Fm, 87.68.+z

## I. INTRODUCTION

Magnetic particles in the nanometer range possess increasing importance as diagnostic and therapeutic tools in medicine, as well as in cellular biology [1–3]. *In vitro*, magnetic forces are used to track and separate magnetically labeled cells or targeted organelles and are involved in a wide variety of magnetic immunoassays [4]. *In vivo*, performing magnetic resonance imaging (MRI), the presence of magnetic nanoparticles (MNP) in tissue of interest results in contrast variations by modifying the proton relaxation parameters [5]. The combination of magnetic nanoparticles with biologically active molecules, such as proteins, peptides, receptor ligands or antibodies builds the most promising concepts of biomedical applications. The binding of a biological effector on the MNP offers the opportunity to target efficiently specific receptors of the cell (with applications in intracellular organelles purification for instance) [6,7], specific cells (cell sorting) [8] and thus specific anatomical sites (increasing MRI diagnostic sensitivity and specificity) [9]. One approach to improve functional imaging is to graft monoclonal antibody to MNP in order to induce receptor mediated uptake in targeted cells as for instance tumor cells [10]. A recent MRI study takes advantage of the targeting ability and the produced signal amplification to image *in vivo* an exogeneous gene expression [11]. The targeting efficiency grounds on one part on a stable link between the active substance and the MNP and on the preservation of the effector functionality, and on the other part on nonspecific factors such as the complex size, charge, and surface modifications that affect the interactions with cells and further the clearance from the circulation, complement fixation, adherence to phagocytes, and the differential tissue deposition [12].

In this paper, we propose a method based on an optical technique [13] to detect the binding reaction of the biologically active substance on the MNP in colloidal suspension, by characterizing the hydrodynamic size of the complex that is formed. Unlike biological methods based on immunochemical reactions on the unbound effectors, our assay is based on a physical measurement of the size of the formed complex compared to the bare particle and thus does not depend on the nature of the bound effector except via its size in solution. Under an external magnetic field, the magnetic moment of each particle together with its optical axis aligns along the direction of the field: the colloidal suspension acquires a net magnetization and simultaneously an optical birefringence [14], which is measured with the appropriate setup. Switching off the external field, the particles lose their preferential orientation under the effect of their Brownian rotational motion within the carrier fluid. The magnetically induced birefringence (the analogous of the electric birefringence [15,16]) relaxes with a characteristic time that is proportional to the hydrodynamic volume of the particle or of the complex formed by the particle and the grafted biomolecule. We investigate in this work the nonspecific physisorption of a polyclonal antibody on ionic nanoparticles and by comparison on ionic particles previously coated with bovine serum albumin. The birefringence relaxation is measured for different amounts of antibodies involved in the binding reaction. From the analyses of the birefringence relaxation curves, we determine the distribution of the complex sizes for the different conditions. The robustness of the method is proved by comparing samples sorted in size through gel filtration.

 

## II. MATERIALS AND METHODS

### A. Synthesis of the magnetic nanoparticles and binding assay

The aqueous ionic ferrofluid, used in this work, is composed of nanoparticles of maghemite ($\gamma Fe_2O_3$). The magnetic particles bearing surface charges are also macroions and repel each other through electrostatic interaction ensuring the stability of the ferrofluid in aqueous solution. Thus, we obtain stable colloidal suspension without using surfactant. The precursor ionic ferrofluid is synthesized according to the Massart's method [17] by alkalizing an aqueous mixture of iron (II) chloride and iron (III) chloride. The so obtained magnetite ($Fe_3O_4$) particles are then acidified, oxidized in maghemite ($\gamma Fe_2O_3$) and dispersed into water leading to an acidic ferrofluid composed of magnetic particles positively charged with nitrate counterions.

#### *1. DMSA-coated magnetic particles*

According to the process described elsewhere [18], the positively charged particles are chelated with *meso-2, 3-dimercaptosuccinic acid* ([HOOC-CH(SH)]-CH(SH)-COOH) or DMSA, which forms strong complex with the surface layer of the particle. To eliminate the different counterions ($NO_3^-$,$TAM^+$,$Cl^-$) and the free DMSA, the ferrofluid is purified two times by ultrafiltration in a 100 kDa Macrosep filter (Filtron) centrifugated at 3000 rpm during 45 min. One obtains an aqueous sol of thiolated maghemite nanoparticles, which is stable in a large $p$H range (from 3 to 11), in suitable ionic strength ($<0.35$ mol/l) and in various buffers such as hepes. In our study, the DMSA particles are dispersed in hepes 0.1 *M* (Sigma H. 9897) at $p$H 7.5. The surface charges are mainly due to unbound carboxylate groups ($COO^-$). After thiolation, there exists SH groups remaining free on the particle surface that can be used to graft a biological effector to the particle via covalent *S—S* bridge or *S—C* bridge, if the effector is previously activated with heterobifunctional cross-linking reagents [19]. In this paper, however, we study the adsorption of a polyclonal immunoglobuline on the particle surface.

#### *2. BSA-coated magnetic particles*

Bovine serum albumin (BSA) is a single polypeptide chain consisting of about 583 amino acid residues (with an excess of acidic amino acids) and no carbohydrates, with molecular weight 66.4 kDa and isoelectric point about 5. DMSA-particles ($[Fe]=0.2$ *M*) are incubated overnight at 4°C with an aqueous solution containing 0.5% BSA, corresponding to an initial molar ratio $[BSA]/[Particles]=5$. As demonstrated later by the birefringence measurement, BSA is efficiently adsorbed on the DMSA-particles surface.

#### *3. IgG binding assay*

For the binding assay, the antibody is a polyclonal purified bovine (Immunoglobuline G) IgG (Sigma, ref15506) isolated from pooled normal bovine serum and used in a variety of immunoassays. It is chosen for its low price and for its easy adsorption on the particle surface. Different quantities of purified bovine IgG (molecular weight 150 kDa) are added to 1.5 ml of a suspension of DMSA particles and to 1.5 ml of a suspension of BSA-coated particles, both in hepes 0.1 *M*, at $p$H=7.5 and with an iron concentration $[Fe]=0.215$ *M* (measured by atomic absorption). The initial molar ratio $[IgG]/[Particles]$ varies from 0 to 0.96. The mixture is then incubated overnight at 4°C. 0.5 ml of the IgG-ferrofluids is reserved for birefringence measurement.

#### *4. Gel filtration*

Gel filtrations are performed on 1 ml sample in an exclusion chromatography colomn (*Sepharose Gel, CL4B200, Sigma*, length 52 cm, section 0.785 $cm^2$, flow rate 0.24 $cm^3$/min, dead volume 14 $cm^3$, eluant:hepes). The fractionation range of this colomn made of beaded agarose lies between 60 and 20000 kDa for globular proteins. The successive populations are collected using a fraction collector (25 drops each) in 1 ml flasks. The optical density (OD) at 575 nm is measured for each fraction in a 1-cm-thick chamber. It is verified that the OD is directly proportional to the iron concentration, so that the particle content for each fraction is determined. The gel filtration is performed for the samples with DMSA particles.

### B. Characterization of the magnetic nanoparticles

The photographs obtained by transmission electron microscopy show that the magnetic nanoparticles are roughly spherical and polydisperse ($3\ \text{nm}<D_{TEM}<15\ \text{nm}$). They consist of monocrystalline ferrimagnetic monodomain of maghemite ($\gamma Fe_2O_3$, an iron oxide with inverse spinel structure) with a crystallite diameter, calculated from x-ray-diffraction data, of typically $D_{x\text{-}ray}=8$ nm. The magnetic core diameter distribution may be obtained from analyzing the magnetization curve of the aqueous suspension of the particles as described elsewhere [20]. Each magnetic nanoparticle bears a magnetic moment *m* typically of the order of $10^4\mu_B$ ($\mu_B$ is the Bohr's magneton) depending of $d_{mag}$ the magnetic diameter of the particle as

$$m=m_s\frac{\pi d_{mag}^3}{6},$$

where $m_s=3.5\,10^5$ A/m is the saturation magnetization of the grain material. For particles of magnetic moment *m*, the magnetization is a Langevin function of the parameter $\xi=m\mu_o H/k_BT$. Taking into account the polydispersity of the magnetic core diameter, the Langevin function must be weighted by the size distribution to obtain the ferrofluid magnetization as a function of the magnetic field *H*. Experimental magnetization curves are correctly described assuming a log-normal distribution of particle size with a characteristic magnetic diameter $d_{0\,mag}$ and a polydispersity index $\sigma$. For the ferrofluid used in this study, the fit of the magnetization curve gives $d_{0\,mag}=7.2$ nm and $\sigma=0.35$. The mean diameter of the magnetic core is $d_{mag}=d_{0\,mag}\exp(3\sigma^2/2)=8.7$ nm, corresponding to 13700 iron atoms.

### C. Optical birefringence measurements

In the absence of magnetic field, a colloidal suspension of magnetic nanoparticles presents no magnetization and is optically isotropic. Under magnetic field, the ferrofluid exhibits a strong optical birefringence, as well as a net magnetization, which both saturate in high fields. In our ionically stabilized colloid, it is experimentally demonstrated that this macroscopic birefringence is related to the microscopic optical anisotropy of the particles and to their orientation under magnetic field. The physical origin of the particle optical anisotropy is discussed in Ref. [14]: it is attributed to a single grain behavior and correlated to the surface magnetic anisotropy of nanosized maghemite particles that is evidenced in Refs. [21–23]. This uniaxial surface magnetic anisotropy originates from disordering defects in the ferrimagnetic lattice on the particle surface, associated to a slight ellipticity of the particles (of the order of 1.25). For most of the maghemite particles in the ferrofluid used here, the anisotropy energy is of the same order as the thermal energy. In a first approximation, let us assume that the magnetic moment is locked to the crystalline lattice in the easy direction. The magnetic moment being linked to the optical axis, it rotates together with the particle body. As an external magnetic field is applied, the particle magnetic moments and consequently the anisotropy axes tend to align along the field direction and the ferrofluid solution acquires a net magnetization and exhibits a magnetically induced optical birefringence. When the field is switched off, the magnetization and optical birefringence decrease to zero due to the Brownian rotational motion of the particles. The characteristic time for a particle to lose the orientation of its optical axis under the effect of thermal orientational fluctuations writes [24]

$$\tau = \frac{\pi}{6} d^3 \frac{\eta}{k_B T},$$

where $\eta$ is the viscosity of the carrier fluid, $T$ the temperature, $k_B$ the Boltzmann constant, and $d$ the hydrodynamic diameter of the particle. The principle of the experiment is to measure the relaxation of the magnetically induced birefringence to deduce the hydrodynamic diameter of the particles in the ferrofluid [25–27].

The ferrofluid is probed by a laser beam of wavelength $\lambda_0$. The sample behaves as a birefringent plate characterized by a phase lag $\varphi$ related to its birefringence $\Delta n$. $\Delta n$ is defined as $\Delta n = n_{\parallel} - n_{\perp}$, $n_{\parallel}$ being the optical index in the direction of the magnetic field and $n_{\perp}$ the optical index in the perpendicular direction. For a sample of thickness $e$, the phase lag is $\varphi = 2\pi e \Delta n / \lambda_0$. The ferrofluid presents also a weak dichroism, that we neglect here since it is of second order with respect to birefringence [28]. The polarization of the light transmitted by the ferrofluid sample is analyzed using the optical setup of Fig. 1. An He-Ne laser beam ($L$) of weak power ($\approx 5$ mW) and wavelength $\lambda_0 = 632.8$ nm goes through the optical setup constituted by a polarizer ($P$), the sample ($S$), a quaterwave plate ($\lambda/4$), an analyzer ($A$), and a photodetector (PD). The ferrofluid sample is put in a nonbirefringent glass chamber (thickness $e = 200$ $\mu$m) and submitted to a pulsed vertical magnetic field ($H_p = 12$ kA/m) produced by Helmholtz's coil (HC). The respective directions of polarizer, analyzer, and $\lambda/4$ plate are indicated in the Fig. 1(a). When the magnetic field is switched on, the ferrofluid presents a phase lag $\varphi$ and the light intensity $I(t)$ detected by the photodetector increases towards a saturation value $I_0$. The field is thus switched off with a characteristic time lower than 200 ns and the decrease of transmitted light is observed as illustrated in the part b of Fig. 1(b). The signal is averaged by repeating the sequence of magnetic field pulse in order to obtain a good accuracy to evaluate the baseline. The overall response time of the apparatus is of the order of 1 $\mu$s. As demonstrated elsewhere [29], the transmitted intensity $I$ is proportional to $\varphi$ in the limit of small phase lag $\varphi$ (that is verified for the low iron concentration and chamber thickness used in this study), and thus proportional to $\Delta n$. As shown in Fig. 1(c), the relaxation of $I(t)/I_0$ is not a single exponential, but is correctly described by a stretched exponential law $I(t)/I_0 = \exp[-(t/\tau_0)^{\alpha}]$, $\tau_0$ being a characteristic relaxation time and $\alpha$ characterizing the width of the relaxation time distribution (the smaller $\alpha < 1$, the larger the distribution).

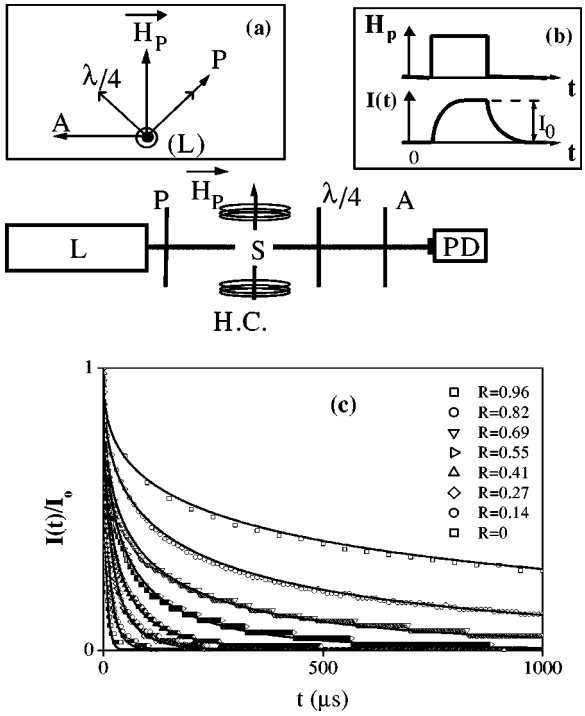


FIG. 1. Experimental setup for the birefringence measurements. Part (a) presents the orientations of the different optical axes. *A*, analyzer; *P*, polarizer; *L*, He-Ne laser; HC, Helmholtz coils; PD, photodetector; *S*, sample. Part (b) shows the pulse of the magnetic field $H_P$ and the corresponding time dependance of transmitted light intensity $I(t)$. $I_0$ is the saturation value of the light intensity under the magnetic field $H_P$. Part (c) shows the time relaxation of the transmitted intensity in linear scale for the ferrofluid (DMSA particles) samples with different ratio $R = [\mathrm{IgG}]/[Particles]$. Plain lines represent the fit of experimental data using stretched exponential law (see Table I for the details of $R$ values and the fit parameters). $t = 0$ corresponds to the switched off of the magnetic field.

TABLE I. Characteristic relaxation times $\tau_0$, hydrodynamic diameters $d_0$, and polydispersity index $\alpha$ as a function of the ratio $R=[\mathrm{IgG}]/[Particles]$ for the DMSA particles as deduced from the fit of experimental intensity transmitted relaxation.

| R | $\tau_0$ ($\mu$s) | $\alpha$ | $d_0$ (nm) |
|---|---|---|---|
| 0 | 5.3±0.2 | 0.86±0.05 | 34.7±0.5 |
| 0.14 | 10.3±0.2 | 0.75±0.02 | 43.3±0.3 |
| 0.27 | 17.2±0.4 | 0.61±0.01 | 51.3±0.4 |
| 0.41 | 25.1±0.5 | 0.55±0.01 | 58.2±0.4 |
| 0.55 | 46.7±0.8 | 0.51±0.01 | 71.5±0.4 |
| 0.69 | 77.6±1.6 | 0.44±0.006 | 84.9±0.6 |
| 0.82 | 184.7±2.4 | 0.43±0.003 | 113.0±0.5 |
| 0.96 | 673.7±13.5 | 0.42±0.005 | 173.9±1.1 |

## III. RESULTS

### A. IgG adsorption on DMSA particles

#### *1. Samples with different initial [IgG]/[Particles] ratios*

Birefringence measurements are performed on all IgG ferrofluid with $[\mathrm{IgG}]/[Particles]$ initial ratio $R$ from 0 to 0.96. The birefringence relaxations for these different samples are represented in Fig. 1(c). Stretched exponential law fits with a very good agreement the experimental relaxation for each sample. One can remark the slowering of the birefringence decay as the number of available IgG per particle is increased. Table I summarizes the parameters $\tau_0$ and $\alpha$ with their standard errors deduced from the fit, and the corresponding hydrodynamic diameter $d_0$ according to the expression of relaxation time for the birefringence $\tau_0 = \pi/6 d_0^3 (\eta/(k_B T))$. Note the tiny values of standard errors for each sample. Figure 2 presents the evolution of $d_0$ and $\alpha$ as a function of the ratio $R$. The initial ferrofluid ($R=0$) has a characteristic hydrodynamic diameter of 34.7 nm and a polydispersity index $\alpha=0.86$. Adding the IgG, the hydrodynamic diameter increases linearly with the ratio $R$ until $R=0.41$. For $R\geqslant 0.55$. the hydrodynamic size grows dramatically reflecting the onset of particle agregation. Consistently with the size increase, the polydispersity is enhanced together with the IgG adsorption. The size and polydispersity growths

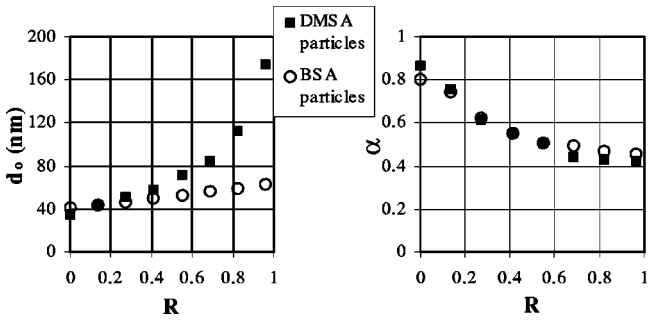


FIG. 2. Characteristic hydrodynamic diameter $d_0$ and polydispersity index $\alpha$ as a function of the ratio $R=[\mathrm{IgG}]/[Particles]$ for the DMSA particles (plain square) and for the BSA-coated particles (empty circles) as deduced from the fit of experimental transmitted intensity relaxation.

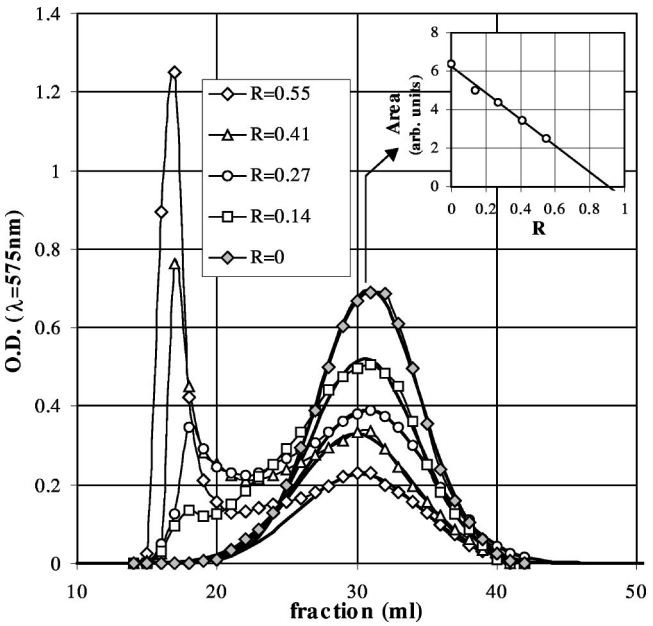


FIG. 3. Optical density (OD) at 575 nm for each successive fraction (1 ml) collected after gel filtration for the samples with different $R$. The first fractions contain the larger particles. Gaussian distributions in the fraction range 20–42 ml [representing the bare particles (see the text)] are shown by bold lines. The area under the Gaussian is plotted in the inset as a function of $R$. Note that assuming a linear extrapolation, this area cancels for $R$ close to 1.

reflect first the IgG adsorption on particles surface for $R \leqslant 0.55$ and second for $R>0.55$, the formation of complex aggregates probably due to the crosslinking of antibodies fixed to the particles.

#### *2. Samples with different initial [IgG]/[Particles] ratios after fractionation by gel filtration*

The samples with $0\leqslant R\leqslant 0.55$ were separated by sepharose gel filtration. The separation depends upon the ability of sample particles to enter pores of a stationary phase. Above a certain size (the exclusion limit is 20 000 kDa for globular proteins), the particles move equally fast and no separation occurs : it corresponds to the first fractions collected ($fraction<14$ ml). Below the exclusion limit, particles of decreasing size move at slowering rates and separation occurs ($14\leqslant fraction\leqslant 42$ ml). Thus the successive collected fractions correspond to decreasing particle sizes. The OD at 575 nm, providing the iron concentration, is measured for each fraction and reported on Fig. 3 for samples with various $R$. The initial ferrofluid ($R=0$) shows a single peak distribution contained in the later fractions with efficient fractionation. For samples with increasing IgG contents, the distribution is enriched in the faster fractions and thus larger particle sizes and a second peak is growing. The conservation of total particles concentration is verified.

Birefringence measurements were performed on all the fractions of samples with $R=0$, 0.14, 0.27, 0.41, and 0.55. Figure 4 shows the evolutions of $d_0$ and $\alpha$ for the successive collected fractions. Consistently with the chromatography separation with respect to the particle size, the later is the

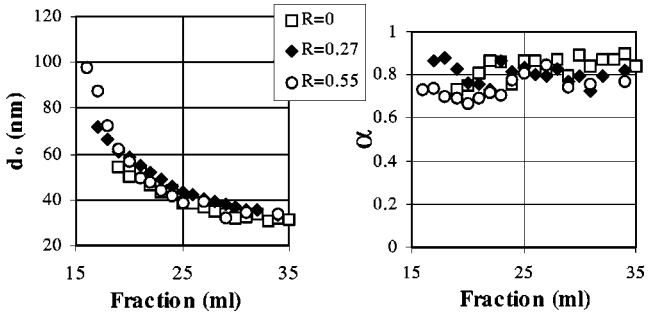


FIG. 4. Characteristic hydrodynamic diameter $d_0$ and polydispersity index $\alpha$ as a function of the fraction collected after gel filtration of the DMSA particles with $R=0$, $R=0.27$, and $R=0.55$.

fraction, the smaller the hydrodynamic diameter is found. For a given $R$, the polydispersity index $\alpha$ does not vary notably for the different fractions and remains always smaller for each fraction ($\alpha \approx 0.8$) than for the nonfractionated ferrofluid. It demonstrates the efficiency of the size separation as well as of the distribution determination by the birefringence experiment. In the first fractions, one observes an increase of the particle size and the polydispersity as $R$ is incremented. By contrast, for the later fractions, the birefringence measurements give approximatively the same characteristic diameters and polydispersity index for all ratios $R$. This can be explained by the fact that the first fractions being nonselective contain all particles above a typical size corresponding to the exclusion limit, while the particles sorting is effective for the later fractions. In the range of efficient fractionation, the diameter and polydispersity of each fraction do not depend upon the initial size distribution but only upon the particular type of gel used here in the filtration colomn.

### B. IgG adsorption on BSA-coated particles

For this binding assay, the DMSA particles are previously incubated with BSA and thus in a second step incubated with the IgG. From the birefringence measurement, we obtain for the particles incubated with BSA, $d_0=41.2$ nm and $\alpha=0.8$ to be compared to the bare DMSA particles in hepes with $d_0=34.7$ nm and $\alpha=0.86$. These differences demonstrate an efficient coating of BSA on the particle surface. Adding more than one IgG per BSA-coated particle, no flocculation is observed. As shown in Table II and illustrated in Fig. 2, the hydrodynamic diameter $d_0$ is a linear function of $R$ in the whole experimental range by contrast with the IgG adsorption on bare DMSA particles. $\alpha$ is decreasing in the same way that for bare DMSA particles. IgG adsorption on BSA-coated particles shifts of about 21 nm the characteristic particle diameter when one IgG per particle is added. We should see later that, for the IgG of 150 kD molecular weight, the shift of characteristic particle diameter growing from 0 to 21 nm is consistant with an increasing ratio of BSA-coated particles bearing one IgG.

TABLE II. Characteristic relaxation times $\tau_0$, hydrodynamic diameters $d_0$, and polydispersity index $\alpha$ as a function of the ratio $R=[\mathrm{IgG}]/[\mathrm{BSA}\ Particles]$ for the BSA-coated particles.

| R | $\tau_0$ ($\mu$s) | $\alpha$ | $d_0$ (nm) |
|---|---|---|---|
| 0 | $8.9\pm0.2$ | $0.80\pm0.02$ | $41.2\pm0.3$ |
| 0.14 | $10.7\pm0.2$ | $0.74\pm0.02$ | $43.8\pm0.3$ |
| 0.27 | $12.3\pm0.4$ | $0.62\pm0.02$ | $45.6\pm0.5$ |
| 0.41 | $15.1\pm0.5$ | $0.60\pm0.01$ | $49.6\pm0.5$ |
| 0.55 | $18.8\pm0.7$ | $0.50\pm0.01$ | $52.8\pm0.7$ |
| 0.69 | $22.8\pm0.8$ | $0.51\pm0.01$ | $56.4\pm0.7$ |
| 0.82 | $26\pm0.9$ | $0.47\pm0.01$ | $59.0\pm0.7$ |
| 0.96 | $30.9\pm2.6$ | $0.45\pm0.02$ | $62.5\pm1.7$ |

## IV. DISCUSSION

### A. From birefringence relaxation measurements to particle size distribution

In our experiments, the birefringence relaxation is satisfactory adjusted using a stretched exponential $I(t)/I_0=\exp[-(t/\tau_0)^{\alpha}]$. This expression is commonly used in a wide variety of system from condensed to soft matter (spin glasses [30], complex liquids [16]) if nonexponential time relaxation are observed. This phenomenological behavior is often attributed to the effect of a large distribution of relaxation times [30]. The shape of this distribution can, in principle, be deduced from a fit to the experiments. Assuming a distribution of relaxation time $\tau$ with a probability density $Q(\ln\tau)$, the time dependence of the birefringence can be written as

$$I(t)=\int I_o(\tau)\exp(-t/\tau)Q(\ln\tau)d(\ln\tau).$$

Let us do approximations to derive analytically the probability density $Q(\ln\tau)$. We neglect in a first time the dependance on $\tau$ of the static birefringence of a particle, $I_0(\tau)\simeq I_o$. This dependance is here weak in front of the sharp variations with $\ln\tau$. Those variations are so sharp that we can split up the integral into two parts. The first part concerns the particles with relaxation times $\tau<t$, their birefringence having relaxed during the time $t$ so that the exponential can be approximated by zero. The second part concerns the particles with relaxation times $\tau>t$, which preserves at the time $t$ the memory of their birefringence: the exponential can be approximated by unity. Within this cutoff approximation, $I(t)/I_0$ can be rewritten as

$$I(t)/I_0=\int_{\tau>t}Q(\ln\tau)d(\ln\tau)=\int_{\ln t}^{\infty}Q(\ln\tau)d(\ln\tau).$$

It follows that

$$Q(\ln t)=-\frac{d[I(t)/I_0]}{d(\ln t)}.$$

The stretched exponential $I(t)/I_0=\exp[-(t/\tau_0)^{\alpha}]$ fits with a good agreement the experimental relaxations: the corre-

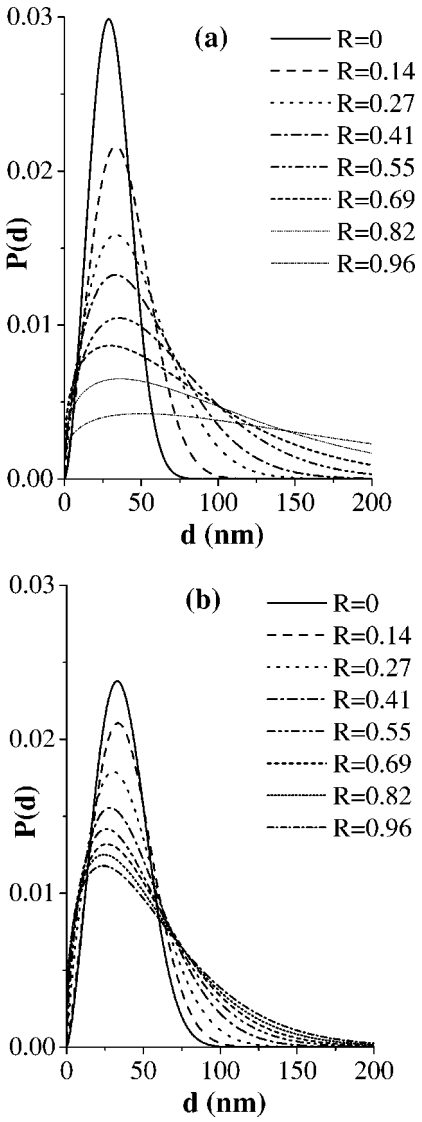


FIG. 5. Distribution of hydrodynamic diameters of the samples with increasing ratio $R=[\mathrm{IgG}]/[Particles]$ for DMSA particles (a) and BSA-coated particles (b).

sponding relaxation time distribution can be written analytically within the cutoff approximation,

$$Q(\ln\tau)=\alpha\left(\frac{\tau}{\tau_0}\right)^{\alpha}\exp\left[-\left(\frac{\tau}{\tau_0}\right)^{\alpha}\right].$$

The probability density for a particle hydrodynamic diameter $d$ writes $P(d)=3/dQ(\ln\tau)$.

### B. Particle size distributions

#### *1. IgG adsorption on DMSA particles and on BSA coated particles*

To reveal the IgG adsorption on DMSA particles and on BSA-coated particles, the diameter distributions found for each value of $R$ are represented in Fig. 5, comparatively for both types of particles. For $R=0$, the size distribution is slightly shifted and widened after BSA adsorption, five BSA per particle being available during adsorption. At physiological $p$H and ionic strength, BSA appears on electron photomicrographs as an oblate ellipsoid with a major axis of 6 nm and a minor axis of 4.5 nm [31]. Small angle neutron scattering study of BSA solution (1% BSA) [32] reports hard sphere diameter of 6.9 nm. Besides, an hydrodynamic diameter of 7.2 nm is deduced from the measurement of translational diffusion coefficient by quasielastic light scattering [33]. A recent study [34] claims in favor of a rigid conformation of BSA in neutral solution with a heart shape structure. From the measurement of the birefringence relaxation due to rotational diffusion, we find a shift of 6.5 nm on the characteristic particle diameter. This shift is consistent with the adsorption of BSA proteins on the particle surface. The slight widening of the diameter distribution suggests that particles may have adsorbed inhomogeneously one or several BSA molecules.

Adding the IgG, the evolution of the diameter distributions with increasing $R$ are qualitatively different for DMSA particles and for BSA-coated particles. As noted before, in the case of DMSA particles, the distributions are enlarged as $R$ is increased, first because of IgG adsorption on the particle surface, but mainly by the fact of particle agregates formation for $R>0.55$. By contrast, for the same value of $R$, BSA-coated particles present relatively narrow distributions, which evidence the absence of particle agregation. These different behaviors with respect to the particle aggregation very probably originate from the different surface coatings. The spontaneous dimerization of antibodies may induce the aggregation of DMSA particles by cross-linking antibodies that are simultaneously bound to one particle. On the contrary, the negatively charged BSA proteins adsorbed on the particles surface strengthen the electrostatic repulsion and simultaneously create steric repulsions that are unfair to multiple antibody linking. As a conclusion, the hydrodynamic diameter distribution reflecting the complex size as well as the aggregation state differenciates DMSA particles and BSA-coated particles. These features are important with respect to their interactions with cells: we show in another study that their binding to the cell surface as well as their subsequent uptake were lower by one order of magnitude for BSA-coated particles compared to DMSA particles and diminish with increasing hydrodynamic diameter. Moreover, the coating of particles with albumin reasonably mimics the effect of opsonization (adsorption of serum proteins on the particle surface), when DMSA particles are injected intravenously. Thus the characterization of both types of particles and their behavior with respect to IgG adsorption are crucial for the fate of particles *in vivo* and the targeting efficiency.

#### *2. Separating bare particles and IgG bound particles*

The particle size distributions deduced from birefringence measurement on each fraction obtained after the gel filtration of DMSA particles with $R=0.55$ are illustrated in Fig. 6. The diameter distributions are shifted to lower diameters with increasing collected fractions revealing the performance of gel separation. The particle concentration in each fraction are independently deduced from OD measurements. One can thus reconstruct the particle size distribution of the nonfrac-

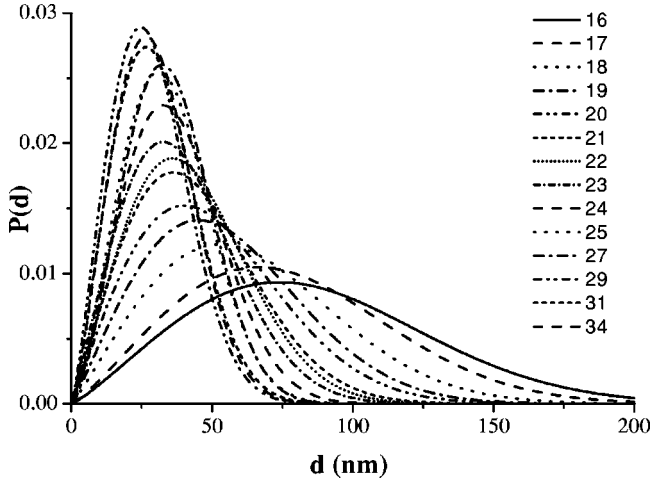


FIG. 6. Distribution of hydrodynamic diameters for the different fractions collected after gel filtration of the DMSA-particles sample with $R=0.55$.

tionated ferrofluid by simply adding the size distributions of each fraction, weighted by the corresponding particles concentrations. Figure 7 shows the remarkable agreement between the so obtained reconstructed distribution and the initial distribution of the nonfractionated ferrofluid for bare particles ($R=0$), and also the satifactory agreement for the ferrofluid incubated with IgG at ratio $R=0.14$, 0.27, and 0.41. Moreover, the birefringence measurements demonstrate the efficiency of the gel separation for a size sorting of the functionalized ferrofluid.

The OD measurements for each fraction of the native ferrofluid ($R=0$) (see Fig. 3) show that the bare particles are distributed in the fractions between 20 and 42 ml. Moreover, the OD distribution as a function of the collected fraction is correctly adjusted for $R=0$ by a Gaussian distribution. For

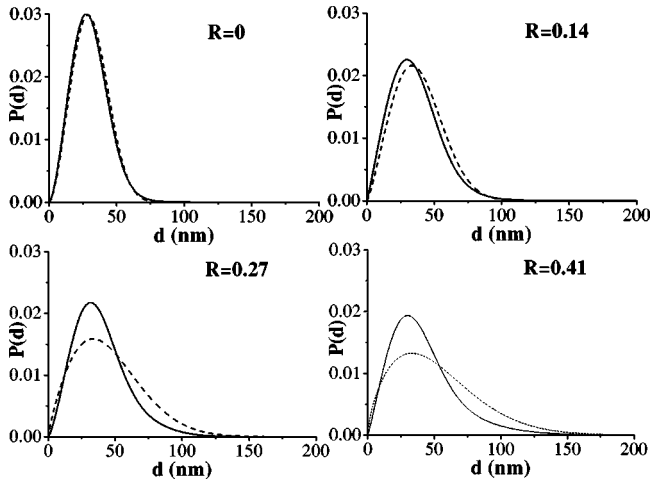


FIG. 7. Comparison of the diameter distribution obtained for the ferrofluid sample before gel filtration (plain line) and the diameter distribution reconstructed as the sum of the distribution of each fraction collected after gel filtration (dotted line) weighted by their respective iron concentration for $R=0$, $R=0.14$, $R=0.27$, and $R=0.41$.

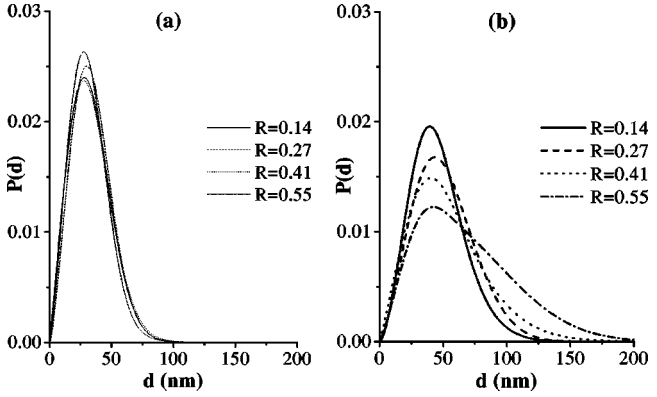


FIG. 8. Diameter distributions of the bare particles (a) and IgG bound particles (b) for $R=0,0.14,0.27,0.41$, and 0.55 reconstructed as sum of distributions of different collected fractions with their respective weight (see the text for the detail of reconstruction).

$R>0$, we assume that particles that are not bound to the IgG keep their native diameter and contribute to the OD distribution on the form of a Gaussian distribution in the fraction range 20–42 ml, which fits the right part of the OD curve (fractions >28 ml). These Gaussian distributions are plotted in Fig. 3 in bold lines, representing the population of bare particles for each sample with different *R*. The area under the Gaussian distribution measures the proportion of bare particles: the inset of Fig. 3 shows that this proportion decreases linearly with increasing *R*. Assuming a linear extrapolation, one can remark that the proportion of bare particles vanishes for $R\simeq 1$ suggesting that each IgG bound particle bears only one IgG. Actually this theoretical limit is not attained experimentally since we observe for $R>0.55$ particles aggregation, which probably occurs via antibody dimerization. However, the linear decrease of the proportion of bare particles canceling at $R\simeq 1$ suggests that for $R<0.55$, an IgG bound particle may bear only one IgG.

We know for each fraction the weight of bare particles (defined by the Gaussian contribution to the OD) and the complementary weight of IgG bound particles. It is thus possible to reconstruct separately on one side the diameter distribution of the bare particles and on the other side the diameter distribution of the IgG bound particles. Figure 8(a) represents the diameter distributions of bare particles for the different *R* reconstructed on the basis of about 20 birefringence relaxation measurements for each *R*. These distributions superimpose remarkably attesting the robustness of the method. Figure 8(b) shows the diameter distribution of IgG bound particles. The binding of the IgG on the particle surface shifts the maximum of size distribution by about 10 nm, the shift being approximatively constant with increasing *R*. Murphy *et al.* [35] have investigated the size parameters of model antigen-antibody complexes formed by the interaction of bovine serum albumin with pairs of monoclonal anti-BSA antibodies by quasielastic light scattering (QLS), classical light scattering (CLS) and electron microscopy. They find radius of gyration (from CLS) and hydrodynamic radius (from QLS) varying from 10 to 20 nm for molecular weights from 400 to 700 kDa depending of the pairs of antibodies binding to different BSA domain. The obtained shift of 10

nm is thus consistent with the polyclonal IgG used in that study molecular weight of about 150 kDa. The most probable diameter of the IgG bound particles is only slightly modified when $R$ increases. It confirms that, on average, only one IgG is attached per particle and that the binding reaction do not induce agregation process in the range $R<0.55$. However, for $R=0.55$, we remark a net widening of the size distribution towards large diameters, signaling the onset of particle aggregate formation.

### C. Conclusion

In this paper, a physical method to detect the binding reaction of macromolecules on magnetic nanoparticles is presented. In a first step, it is shown that the direct analysis of the magnetically induced birefringence relaxation, with the aid of a stretched exponential adjustment, could reveal the binding of a macromolecule on the particle surface and distinguish it from an eventual onset of particle agregation. This field induced birefringence experiment appears as a rapid and simple assay to probe binding reaction on magnetic nanoparticles considered as substrates, which can be applied in a wide variety of *in vitro* process.

As a second step, a quantitative support for the robustness of the method is provided. An analysis of birefringence relaxation permits to deduce the distribution of the hydrodynamic diameter of the complex formed by the nanoparticles and attached macromolecules. Besides, thanks to a gel filtration, a size fractionation of samples with increasing IgG per particles ratio is performed. It unambiguously confirms the sensitivity of the proposed birefringence method to derive particle diameter distributions. Finally, on the basis of birefringence measurements on fractionated samples, it is possible to separate the distribution of bare particles from the distribution of IgG bound particles in order to obtain more quantitative results on the efficiency of the binding reaction.

Birefringence measurements point out the different behavior of DMSA particles and BSA-coated particles with respect to the IgG adsorption. As the complex size, the number and conformation of adsorbed IgG and the cluster formation are important factors for their interactions with cells, their characterizations by birefringence measurement are crucial for the choice of particles, determining the fate *in vivo* and the possibility of targeting.

From a biomedical point of view, the certainty that magnetic nanoparticles effectively bear a biological effector is the first step towards a wide variety of applications. In the field of cell biology, functionalized nanoparticles can be driven into intracellular compartments (lysosomes, reticulum, golgi apparatus), following the grafted antibody pathway. It then becomes possible to apply magnetic forces inside the cell and to displace one type of organelle. For medical diagnosis and therapy, specific antibodies or other effectors grafted on magnetic nanoparticles allow to detect the presence of a receptor in an analyte *in vitro* and to target analytical sites *in vivo*.

### ACKNOWLEDGMENTS

This work was supported by the ACI No. 166 (télémédecine et technologie pour la santé) from the Ministère de la Recherche and by the Centre National de la Recherche Scientifique. We gratefully acknowledge J. Browaeys for his advice and fruitful discussions and J. Servais for his technical assistance.

[1] W. Schütt C. Grüttner, U. Häfeli, M. Zborowski, J. Teller, H. Putzar, and C. Schümichen, Hybridoma **16**, 109 (1997).
[2] J. Roger, J.N. Pons, R. Massart, A. Halbreich, and J.-C. Bacri, Eur. Phys. J.: Appl. Phys. **5**, 321 (1999).
[3] Proceedings of the Third International Conference on Scientific and Clinical Applications of Magnetic Carriers, edited by U. Häfeli and H. Zbozowski [J. Magn. Magn. Mater. **225**, 1 (2001)].
[4] Y.R. Chemla, H.L. Grossman, Y. Poon, R. McDermott, R. Stevens, and J. Alper Clarke, Proc. Natl. Acad. Sci. U.S.A. **97**, 14 268 (2000).
[5] R. Weissleder and P. Reimer, Eur. J. Radiol. **3**, 198 (1993).
[6] L.A. Perrin-Cocon, P.N. Marche, and C.L. Villiers, Biochem. J. **338**, 123 (1999).
[7] A.P. Kausch, T.P. Owen, Jr., S. Narayanswami, and B.D. Bruce, BioTechniques **26**, 336 (1999).
[8] K.E. McCloskey, J.J. Chalmers, and M. Zborowski, Cytometry **40**, 307 (2000).
[9] M. Lewin, N. Carlesso, C.H. Tung, X.W. Tang, D. Cory, D.T. Scadden, and R. Weissleder, Nat. Biotechnol. **18**, 410 (2000).
[10] A. Moore, E. Marecos, A. Bogdanov, Jr., and R. Weissleder, Radiology **214**, 568 (2000).
[11] R. Weissleder, A. Moore, U. Mahmood, R. Bhorade, H. Benveniste, E.A. Chiocca, and J.P. Basilion, Nat. Med. **6**, 351 (2000).
[12] D. Hogemann, L. Josephson, R. Weissleder, and J.P. Basilion, Bioconjugate Chem. **11**, 941 (2000).
[13] G. Gerald Fuller, *Optical Rheometry in Complex Fluids* (Oxford University Press, Oxford, 1995).
[14] E. Hasmonay, E. Dubois, J.C. Bacri, R. Perzynski, Yu.L. Raikher, and V.I. Stepanov, Eur. Phys. J. B **5**, 859 (1998).
[15] B.R. Jennings and D.M. Oakley, Appl. Opt. **21**, 1519 (1982).
[16] V. Degiorgio, R. Piazza, F. Mantegazza, and T. Bellini, J. Phys.: Condens. Matter **2**, SA69 (1990).
[17] R. Massart, IEEE Trans. Magn. **17**, 1247 (1981).
[18] N. Fauconnier, J.N. Pons, J. Roger, and A. Bee, J. Colloid Interface Sci. **194**, 427 (1997).
[19] A. Halbreich, D. Sabolovic, C. Sestier, D. Geldwerth, J.N. Pons, and J. Roger, EP 847528A1, U.S. Patent No. 6, 150, 181 (2000).
[20] *Magnetic Fluids and Applications Handbook*, edited by B. Berkovski (Begell House, New York, 1996).
[21] F. Gazeau, E. Dubois, M. Hennion, R. Perzynski, and Yu.L. Raikher, Europhys. Lett. **40**, 575 (1997).
[22] F. Gazeau, J.C. Bacri, F. Gendron, R. Perzynski, Yu.L. Raikher,

V.I. Stepanov, and E. Dubois, J. Magn. Magn. Mater. **186**, 175 (1998).
[23] V. Shilov, Yu.L. Raikher, J.C. Bacri, F. Gazeau, R. Perzynski, and V.I. Stepanov, Phys. Rev. B **60**, 11 902 (1998).
[24] H. Benoit, Ann. Phys. (Paris) **12**, 6 (1951).
[25] J.C. Bacri, R. Perzynski, D. Salin, and J. Servais, J. Phys. (Paris) **48**, 1385 (1987).
[26] R. Koetitz, J. Lange, J. Browaeys, R. Perzynski, J.-C. Bacri, V. Ponsinet, and T. Rheinlaender, U.S. Patent No. DE-19938384.7-USA-60/148686-PCT/EP00/07150 (1999).
[27] D. Spoliansky, V. Ponsinet, J. Ferré, and J.P. Jamet, EPJdirect **1**, 227 (2000).
[28] F. Bentivegna, M. Nyvlt, J. Ferré, J.P. Jamet, A. Brun, S. Visnovsky, and R. Urban, J. Appl. Phys. **85**, 2270 (1999).
[29] E. Hasmonay, A. Bee, J.-C. Bacri, and R. Perzynski, J. Phys. Chem. B **103**, 6421 (1999).
[30] B. Castaing and J. Souletie, J. Phys. I **1**, 403 (1991).
[31] E.M. Slayter, J. Mol. Biol. **14**, 443 (1965).
[32] R. Nossal, C.J. Glinka, and S.H. Chen, Biopolymers **25**, 157 (1986).
[33] T. Raj and W.H. Flygare, Biochemistry **13**, 3336 (1974).
[34] M.L. Ferrer, R. Duchowicz, B. Carrasco, J.G. de La Torre, and A.U. Acuna, Biophys. J. **80**, 2422 (2001).
[35] R.M. Murphy, H. Slayter, P. Schurtenberger, R.A. Chamberlin, C.K. Colton, and M.L. Yarmush, Biophys. J. **54**, 45 (1988).